Electronic Supplementary Information for: Shape-controlled anisotropy of superparamagnetic micro-/nanohelices

Alexander M. Leshansky[1], Konstantin I. Morozov[1] and Boris Y. Rubinstein[2]

[1]*Department of Chemical Engineering and Russel Berrie Nanotechnology Institute Technion - IIT, Haifa 32000, Israel*

[2]*Stowers Institute for Medical Research, Kansas City, MO 64110, USA*

(Dated: April 3, 2016)

I. EFFECTIVE CONCENTRATION OF MAGNETIC INCLUSIONS

The susceptibility of the polydisperse random system of magnetic particles with weak and intermediate dipolar-dipolar interaction ($\lambda \leq 3$) is well described by the one-parameter relation [1]:

$$\chi = \chi_L(1 + 4\pi\chi_L/3)\,, \tag{S1}$$

where $\chi_L = \sum_i n_i m_i^2/(3k_BT)$ is the Langevin susceptibility, n_i and m_i are the number concentration and magnetic moment of components of i-sort, respectively.

In our modeling, instead of the polydisperse sample, we consider the monodisperse system with the same value of the Langevin susceptibility χ_L. Of course, the monodisperse system cannot be completely equivalent to the polydisperse one. We will show that the volume fraction ϕ of the effective monodisperse particles is higher then the fraction ϕ_0 of inclusions in the original polydisperse system and the ratio ϕ/ϕ_0 depends on the broadness of the original size distribution of nanoparticles.

Let us consider two characteristic quantities of the polydisperse system – the volume fraction of particles $\phi = \pi n\langle d^3\rangle/6$ ($n = \sum_i n_i$ being the volume concentration of all particles) and the Langevin susceptibility, $\chi_L = n\langle m^2\rangle/(3k_BT)$. Here and below the brackets mean the averaging over the size distribution function $f(d)$ of inclusions. The magnetic moment m_i of the grain of ith type is expressed via particle saturation magnetization M_s and its volume $V_i = \pi d_i^3/6$, $m_i = M_sV_i$. Then we have $\chi_L = \frac{1}{3}(\pi/6)^2(k_BT)^{-1}M_s^2 n\langle d^6\rangle$. Therefore, both parameters are described by the third and sixth moments of the distribution function [2]: $\phi \sim \langle d^3\rangle$ and $\chi_L \sim \langle d^6\rangle$.

For the polydisperse system, the ratio $p = \langle d^6\rangle/\langle d^3\rangle^2 > 1$ and the deviation from unity is determined by the width of the particle distribution. Indeed, let us show this explicitly using an example of the log-normal distribution of particles:

$$f(d) = \frac{1}{\sqrt{2\pi}d\sigma}e^{-\frac{\ln^2(d/d_0)}{2\sigma^2}}\,, \tag{S2}$$

where d_0 and σ are, correspondingly, the characteristic size of the inclusion and the distribution width. The moments of the distribution function (S2) read:

$$\langle d^n\rangle = d_0^n e^{\frac{n^2\sigma^2}{2}}\,. \tag{S3}$$

Thus, the ratio $p = \langle d^6\rangle/\langle d^3\rangle^2 = e^{9\sigma^2}$, i.e., the wider the distribution, the higher values of p. Only for monodisperse system with $\sigma = 0$ one has the ratio $p = 1$.

In our numerical scheme we replace the polydisperse system by the monodisperse one, while keeping the Langevin susceptibility χ_L to be constant. This corresponds to the particle size d_{mono} of inclusions of the model system $d_{mono} = \langle d^6 \rangle^{1/6}$. This means the increase of the volume fraction ϕ of the model monodisperse system in comparison with its initial value ϕ_0 by the factor

$$\phi/\phi_0 = \langle d^6 \rangle^{1/2} / \langle d^3 \rangle = \sqrt{p} = e^{4.5\sigma^2} \, . \tag{S4}$$

The realistic composites are strongly polydisperse and represented by individual nanoparticles and their agglomerates/aggregates. For example, the resulting size distribution in polymer composites in [3] was quite broad ($\sigma = 0.25$) with a peak at ~ 11 nm corresponding to a single particle, however there was a significant portion of agglomerates which are larger, $d \sim 40$–50 nm, extending up to 80 nm. The particle distribution in Ref. [3] was fitted to bimodal (bi-lognormal) distribution. A rough account of agglomerates within the framework of the one-mode log-normal distribution (S2) shifts the standard deviation to higher values, $\sigma \approx 0.4$. As follows from Eq. (S4), it corresponds to roughly doubling of the effective volume fraction of inclusions, $\phi/\phi_0 \approx 2$.

II. GEOMETRY OF MICRO-/NANOHELICES AND SHAPE PARAMETRIZATION

In this work we consider two types of helical shapes. The first type corresponds to helices with an *elliptical* cross-section of the filament with semi-axis a having a fixed component along the helical axis, and semi-axis b oriented normally to the helical axis. In particular, *normal* helices with the cross-section elongated in the direction transverse to the helical axis ($b > a$), and *binormal* helices with longer cross-sectional axis having a fixed component along the helical axis ($a > b$), while *regular* helices correspond to circular filament cross-section with $a = b$.

In the body-fixed coordinate frame $x_1 x_2 x_3$ with the helix axis oriented along x_3, the equation for the helix centerline can be written in the following parametric representation [5]

$$\boldsymbol{X}(s) = \left[\frac{\kappa}{\lambda^2} \cos(\lambda s), \frac{\kappa}{\lambda^2} \sin(\lambda s), \frac{\tau}{\lambda} s \right] \, . \tag{S5}$$

Here s is the arc length and $\lambda = 1/\sqrt{R^2 + \frac{P^2}{4\pi^2}}$. Curvature κ and torsion τ are defined via

helix radius R and pitch P as $\kappa = R\lambda^2$, $\tau = \frac{P}{2\pi}\lambda^2$, while the helix angle Θ is determined according to the relation $\tan\Theta = \kappa/\tau = 2\pi R/P$. We also mention the following simple relations for the helix angle: $\sin\Theta = \kappa/\lambda = R\lambda\,,\ \cos\Theta = \tau/\lambda = \frac{P}{2\pi}\lambda$.

Let $\{\widehat{\boldsymbol{d}}_1, \widehat{\boldsymbol{d}}_2, \widehat{\boldsymbol{d}}_3\}$ be the right-handed director basis defined at each position s along the axis of the filament [5]:

$$\begin{aligned}
\widehat{\boldsymbol{d}}_1(s) &= \left[\frac{\tau}{\lambda}\sin(\lambda s), -\frac{\tau}{\lambda}\cos(\lambda s), \frac{\kappa}{\lambda}\right]\,, \\
\widehat{\boldsymbol{d}}_2(s) &= [\cos(\lambda s), \sin(\lambda s), 0]\,, \\
\widehat{\boldsymbol{d}}_3(s) &= \left[-\frac{\kappa}{\lambda}\sin(\lambda s), \frac{\kappa}{\lambda}\cos(\lambda s), \frac{\tau}{\lambda}\right]\,.
\end{aligned} \tag{S6}$$

$\widehat{\boldsymbol{d}}_3 = \partial\mathbf{X}(s)/\partial s$ is the vector tangent to the centreline of the filament. Vectors $\widehat{\boldsymbol{d}}_1$ (binormal) and $\widehat{\boldsymbol{d}}_2$ (normal) are assumed to be parallel, correspondingly, to the semi-axes of the filament cross-section (e.g. for the normal helix $\widehat{\boldsymbol{d}}_1$ and $\widehat{\boldsymbol{d}}_2$ are parallel to the short and the long semi-axis, respectively).

Surface parametrization of a helix with elliptic cross-section in the plane formed by the normal and binormal vectors (i.e. normal or binormal and also regular helices, see Figs. 3A–C) reads

$$\boldsymbol{S}(s,u) = \boldsymbol{X}(s) + (a\cos u\ \widehat{\boldsymbol{d}}_1 + b\sin u\ \widehat{\boldsymbol{d}}_2),$$

where $0 \le u < 2\pi$.

For computations of the volume fraction ϕ of magnetic inclusions one has to know the volume of the helix. Possible parametrization of the volume enclosed by the surface $\boldsymbol{S}$ is $\boldsymbol{V}(s,u,r) = \boldsymbol{X}(s) + r(a\cos u\ \widehat{\boldsymbol{d}}_1 + b\sin u\ \widehat{\boldsymbol{d}}_2)$, where $0 \le r \le 1$. Then the differential volume element can be found as

$$\mathrm{d}V = \sqrt{g}\ \mathrm{d}s\ \mathrm{d}u\ \mathrm{d}r,$$

where the jacobian

$$\sqrt{g} \equiv \det\left[\frac{\partial(V_1, V_2, V_3)}{\partial(s,u,r)}\right] = ab(1 + br\kappa\sin u)\,.$$

The volume of the one-turn helix can now be found by the integration of $\mathrm{d}V$ as

$$V = \int_0^{2\pi/\lambda}\mathrm{d}s\int_0^{2\pi}\mathrm{d}u\int_0^1\sqrt{g}\mathrm{d}r = \frac{2ab\pi^2}{\lambda}\,, \tag{S7}$$

where it can be readily shown to be equal to volume of the "straightened" elliptic cylinder i.e. $V = \pi abL$, where $L = 2\pi/\lambda = 2\pi R/\sin\Theta$ is the length of the single helical turn (along the helical centerline) with Θ being the helix angle.

The microhelices fabricated from magnetic polymer composite (MPC) in [4] had elliptic cross-section with fixed orientation of semi-axis a and b in the plane x_1x_2 transverse to the helical x_3-axis (see Fig. S1). Surface parametrization of MPC helix then reads

$$\boldsymbol{S}^{\mathrm{MPC}}(s,u) = \boldsymbol{X} + (a\cos u\,\widehat{\boldsymbol{e}}_1 + b\sin u\,\widehat{\boldsymbol{e}}_2)\,, \tag{S8}$$

where $\widehat{\boldsymbol{e}}_1$ and $\widehat{\boldsymbol{e}}_2$ are the unit vectors along x_1 and x_2 respectively.

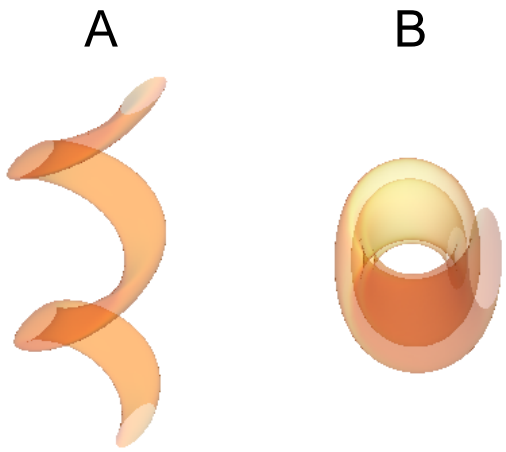

FIG. S1. Illustration of MPC helical micropropeller with two full turns, $R/r = 1.25$, $\Theta = 60°$ (no magnetic inclusions are shown). The filament cross-section aspect ratio (in x_1x_2-plane) is $a/b = 3$; (A) front view; (B) top view (i.e., as viewed along the helical axis).

The volume of MPC helices can be easily found using the Cavalieri's principle, i.e. its volume is equal to the volume of straight elliptic cylinder with cross-section area πab and of the length equal to the length of the helix measured along the x_3-axis, $P = 2\pi R/\tan\Theta$. Thus, the volume of the one-turn helix can be calculated as

$$V = 2ab\pi^2 P = \frac{2ab\pi^2\tau}{\lambda^2} = ab\pi L\cos\Theta\,,$$

where, as before, $L = 2\pi R/\sin\Theta$ is the length of the single turn along the helical centerline.

III. EFFECTIVE MAGNETIZATION OF HELICES: SLENDER BODY THEORY

The slender body (SB) approximation assumes that locally a helical filament can be considered as a thin straight cylinder. We first present the analysis in Ref. [5] for the case of

an *elliptical* cross-section of the filament with semi-axis a along $\widehat{\boldsymbol{d}}_1$ and semi-axis b along $\widehat{\boldsymbol{d}}_2$, i.e. regular, normal and binormal helices, and then apply the theory for MPC helices with elliptic cross-section with fixed orientation of semi-axis a and b in the plane x_1x_2 transverse to the helical axis (see the previous section for details of parametrization). Assumption of slenderness applies to helices with typical dimensions, i.e. the radius R and the pitch P, satisfying $R,\, P \gg \max(a, b)$.

The magnetic susceptibilities of an elliptic cylinder along the three principal axes read [6]

$$\chi_1 = \frac{\chi_0}{1 + 4\pi\chi_0 N_1}\,, \quad \chi_2 = \frac{\chi_0}{1 + 4\pi\chi_0 N_2}\,, \quad \chi_3 = \chi_0\,. \tag{S9}$$

Here N_1 and $N_2 = 1 - N_1$ are the demagnetizing factors along the axis $\boldsymbol{d}_1$ and $\boldsymbol{d}_2$, respectively, and we also assumed the zero value of the demagnetizing factor along the long axis of cylinder, $N_3 = 0$. The demagnetizing factor N_1 can be found as [7]:

$$N_1 = (2\pi)^{-1}\left[4\arctan\left(\frac{b}{a}\right) + \frac{2a}{b}\ln\left(\frac{a}{b}\right) + \left(\frac{b}{a} - \frac{a}{b}\right)\ln\left(1 + \frac{a^2}{b^2}\right)\right].$$

The demagnetizing factor N_2 can be found either by the permutation $a \leftrightarrow b$ or from $N_2 = 1 - N_1$. For the regular helix with circular cross-section $N_1 = N_2 = 1/2$.

Eqs. S9 imply that in the external magnetic field helical segments are polarized differently along the principal axes: the easy direction is along the centerline, and the hard one is along the shorter cross-section. This property leads to the apparent anisotropy of magnetic susceptibility $\boldsymbol{\chi}$ of the helix as a whole.

The SB approximation is the *local* theory: the magnetization of each segment is determined only by its geometry and by the applied magnetic field (see Eq. (S1)). In other words, in the framework of SB approximation different parts of the helix do not interact, i.e. magnetize independently from each other. Therefore, the effective susceptibility $\boldsymbol{\chi}$ of helix proves to be an additive property and can be determined by integration

$$\boldsymbol{\chi} = L^{-1}\int_0^L \left(\chi_1\widehat{\boldsymbol{d}}_1\widehat{\boldsymbol{d}}_1 + \chi_2\widehat{\boldsymbol{d}}_2\widehat{\boldsymbol{d}}_2 + \chi_3\widehat{\boldsymbol{d}}_3\widehat{\boldsymbol{d}}_3\right) ds\,, \tag{S10}$$

where L is the helix length along the centerline.

Let us denote the eigenvalues of matrix $\boldsymbol{\chi}$ in the descending order as $\chi_1 \geq \chi_2 \geq \chi_3$. Generally, all three eigenvalues are different and helix possesses bi-axial magnetization. However, for the *integer* number of turns, the susceptibility tensor S10 becomes *uniaxial*: two out of three eigenvalues coincide. The direct integration in Eq. (S10) using Eqs. (S9)-(S6)

demonstrates that the eigenvectors of $\boldsymbol{\chi}$ are aligned with the BCS axes $x_1x_2x_3$; the magnetic anisotropy parameter $\Delta\chi$, defined as the difference of eigenvalues along the anisotropy (i.e. helical) axis and in transverse direction, $\Delta\chi = \chi_{\parallel} - \chi_{\perp}$, reads

$$\Delta\chi = \frac{1}{2}[(\chi_3 - \chi_1)(3\cos^2\Theta - 1) + \chi_1 - \chi_2]\,. \tag{S11}$$

Particularly simple form of magnetic anisotropy parameter can be obtained for the case when $4\pi\chi_0 \ll 1$. Taking the asymptotic small-χ_0 limit of susceptibilities in Eqs. (S9), $\Delta\chi$ in Eq. (S11) can be further simplified into

$$\frac{\Delta\chi}{2\pi\chi_0^2} = 1 - 3N_1\sin^2\Theta\,. \tag{S12}$$

The obtained result (S12) indicates that magnetically, integer-number-of-turns helix is equivalent to a polarized spheroid with its easy-axis aligned along the helical x_3-axis. The slender helices with a small pitch angle $\Theta < \Theta_*$ are characterized by the positive value of the anisotropy parameter $\Delta\chi$ (i.e. equivalent to prolate spheroid), whereas for the tight helices with high values of $\Theta > \Theta_*$ the anisotropy parameter becomes negative (i.e. equivalent to oblate spheroid or disk). The critical helix angle Θ_* at which $\Delta\chi$ changes sign is found from the relation $\sin\Theta_* = (3N_1)^{-1/2}$. It is depicted in the inset to Fig. S2 as a function of the aspect ratio a/b of the filament cross-section. For regular helix with a circular cross-section, $a = b$, $\Theta_*^{\mathrm{r}} = 54.7^\circ$. The values of the critical angle Θ_* for the normal and binormal helices prove to be *strongly asymmetric* relatively to its value for regular helix. For example, for $a/b = 2$, $\Theta_*^{n} = 45.8^\circ$ and $\Theta_*^{\mathrm{bn}} = 76.6^\circ$ for the normal and binormal helices, respectively. The minimal value of this critical angle for the normal helix with infinitely thin filament cross-section ($a/b \to 0$) is $\Theta_*^{\mathrm{n}} = 35.3^\circ$, whereas for the binormal helix it reaches it maximal value $\Theta_*^{\mathrm{bn}} = 90^\circ$ already for aspect ratio $a/b \simeq 2.2$. The angle Φ formed by the main eigenvector (corresponding to the maximal eigenvalue χ_1) of the susceptibility tensor and the helix axis is depicted in Fig. S2 as a function of the helix angle Θ for regular (red), normal (blue) and binormal (green) helices. As seen, all dependencies are *step-like* functions: $\Phi = \mathcal{H}(\Theta - \Theta_*)$, where $\mathcal{H}(x)$ is the Heaviside function. This idealized solution relies on three simplifying assumptions: (i) local magnetization, (ii) integer number of helical turns and (iii) uniformity of the geometric and magnetic properties of helices. Any violation of (i)–(iii) should lead to deviation from the ideal dependence and to smoothing out of the step-like profile as illustrated in Fig. S2 by the orange line corresponding to a helix with non-integer number turns and as demonstrated by the direct numerical simulations in the main text.

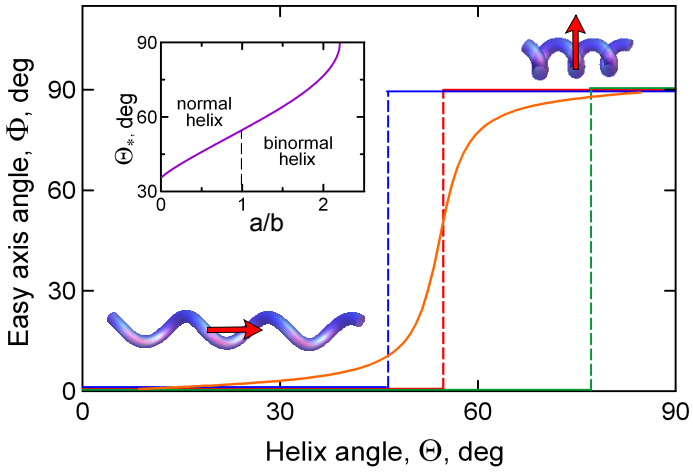

FIG. S2. Inclination angle Φ of the easy-axis as a function of the helix angle Θ for regular (red), normal (blue) and binormal (green) helices with integer number of turns. The aspect ratio of the filament cross-section for normal and binormal helices is $a/b = 0.5$ and 2, respectively. The orange curve, corresponding to a regular helix with 3.3 full turns, illustrates the effect of imperfectness on Φ; the helices and corresponding arrows illustrate the orientation of the easy-axis depending on their slenderness. The inset depicts the critical helix angle Θ_* vs. the filament cross-section aspect ratio a/b.

SB theory can also be applied for estimating the effective magnetization of propellers with more complex geometry, such as, e.g., MPC helices with shape parametrization given by Eq. S8. These helices have elliptical cross-section with fixed orientation of semi-axis a and b in the plane $\{x_1x_2\}$ transverse to the helical x_3-axis. Expanding the unit vectors $\widehat{\boldsymbol{e}}_1$ and $\widehat{\boldsymbol{e}}_2$ in the basis $\widehat{\boldsymbol{d}}_1\widehat{\boldsymbol{d}}_2\widehat{\boldsymbol{d}}_3$ allows to derive the *approximate* parametric representation of the filament cross-section shape in the d_1d_2-plane:

$$
\begin{aligned}
&a\cos u\,\widehat{\boldsymbol{e}}_1 + b\sin u\,\widehat{\boldsymbol{e}}_2 = \\
&\frac{\tau}{\lambda}\left(a\cos u\sin\lambda s - b\sin u\cos\lambda s\right)\widehat{\boldsymbol{d}}_1 + \left(a\cos u\cos\lambda s + b\sin u\sin\lambda s\right)\widehat{\boldsymbol{d}}_2 + (\ldots)\,\widehat{\boldsymbol{d}}_3\,,
\end{aligned}
$$

where only the first two terms are relevant to us. This can also be rewritten as

$$
a\cos u\,\widehat{\boldsymbol{e}}_1 + b\sin u\,\widehat{\boldsymbol{e}}_2 = \widetilde{a}\cos\left(u+\varphi_1\right)\widehat{\boldsymbol{d}}_1 + \widetilde{b}\sin\left(u+\varphi_2\right)\widehat{\boldsymbol{d}}_2 + (\ldots)\,\widehat{\boldsymbol{d}}_3\,, \tag{S13}
$$

where $\widetilde{a} = \frac{\tau}{\lambda}\sqrt{a^2\sin^2\lambda s + b^2\cos^2\lambda s}$, $\widetilde{b} = \sqrt{a^2\cos^2\lambda s + b^2\sin^2\lambda s}$, and $\tan\varphi_1 = (b/a)\cot\lambda s$, $\tan\varphi_2 = (a/b)\cot\lambda s$, showing that the filament cross-section of a slender enough MPC helix in d_1d_2-plane can be accurately approximated by a *tilted* ellipse (see Fig. S3 and [8]).

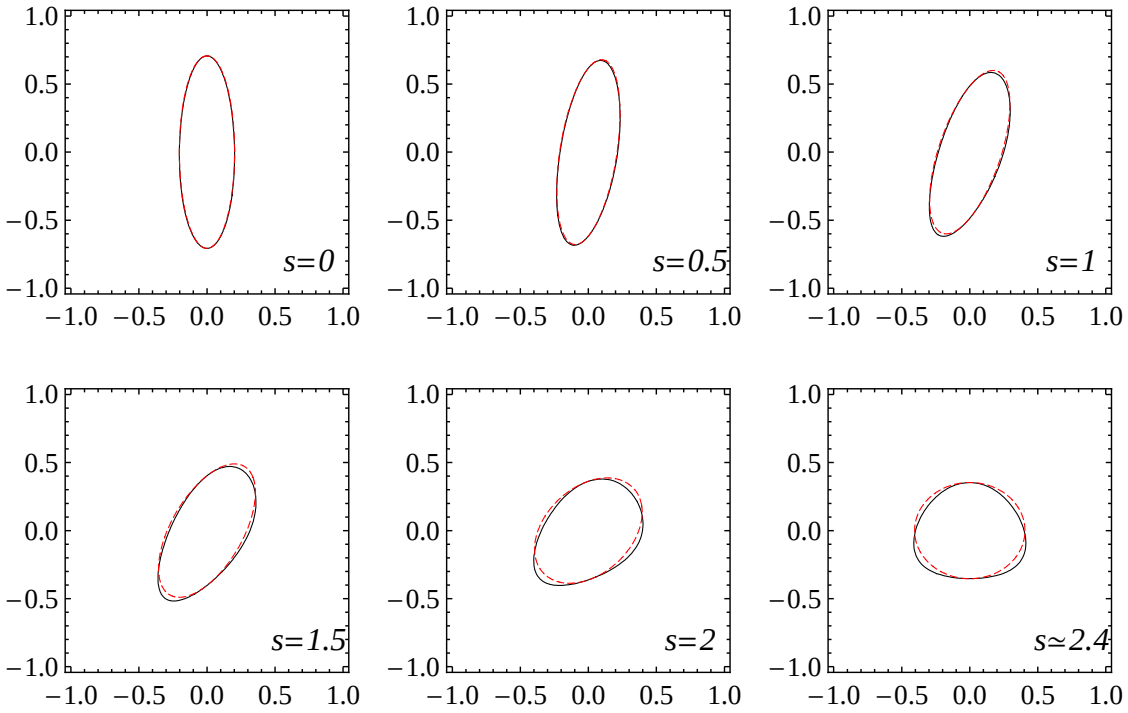

FIG. S3. Filament cross-section in d_1d_2-plane upon varying the parameter $s \in [0, L/4]$ for a MPC helix with radius $R/r = 2.5$ (the equivalent filament radius $r = \sqrt{\pi ab} = 0.5$), helix angle $\Theta = 55^\circ$ and $a/b = 2$. The solid (black) lines are the exact profiles, while dashed (red) lines are the approximate elliptical profiles in S13.

The tilted ellipse can be brought to its canonic form by defining the new variables

$$q_{1,2}\cos\omega_{1,2} = \frac{(\mp a\lambda - b\tau)}{\lambda}\cos\lambda s\,, \quad q_{1,2}\sin\omega_{1,2} = \frac{(\pm a\lambda + b\tau)}{\lambda}\sin\lambda s\,, \tag{S14}$$

we can re-write the parametric form for the filament cross-section as

$$\frac{1}{2}(q_1\sin(u+\omega_1) + q_2\sin(u+\omega_2))\widehat{\boldsymbol{d}}_1 + \frac{1}{2}(-q_1\cos(u+\omega_1) + q_2\cos(u+\omega_2))\widehat{\boldsymbol{d}}_2 = \frac{(q_1+q_2)}{2}\cos t\;\widehat{\boldsymbol{d}}'_1 + \frac{(q_1-q_2)}{2}\sin t\;\widehat{\boldsymbol{d}}'_2\,,$$

where the new parameter $t = u + (\omega_1+\omega_2)/2$ and

$$\widehat{\boldsymbol{d}}'_1 = \widehat{\boldsymbol{d}}_1\cos\vartheta - \widehat{\boldsymbol{d}}_2\sin\vartheta\,, \quad \widehat{\boldsymbol{d}}'_2 = \widehat{\boldsymbol{d}}_1\sin\vartheta + \widehat{\boldsymbol{d}}_2\cos\vartheta\,, \tag{S15}$$

with $\vartheta = (\omega_2 - \omega_1)/2$. Thus, the parametric representation of the filament cross-section in S15 is an ellipse with major, $\widehat{a}$, and minor, $\widehat{b}$, semi-axes equal to $(q_1+q_2)/2$ and $(q_1 -$

$q_2)/2$, respectively, and oriented along rotated (by an angle ϑ as in Eq. S15) axes $(\widehat{\boldsymbol{d}}'_1, \widehat{\boldsymbol{d}}'_2)$, correspondingly.

Now the effective susceptibility can be written in the form

$$\boldsymbol{\chi}^{\mathrm{MPC}} = L^{-1} \int_0^L \left(\chi_1 \widehat{\boldsymbol{d}}'_1 \widehat{\boldsymbol{d}}'_1 + \chi_2 \widehat{\boldsymbol{d}}'_2 \widehat{\boldsymbol{d}}'_2 + \chi_3 \widehat{\boldsymbol{d}}_3 \widehat{\boldsymbol{d}}_3 \right) ds \,, \tag{S16}$$

The effective susceptibility of MPC helices, $\boldsymbol{\chi}^{\mathrm{MPC}}$, is found by numerical integration of Eq. S16 where $\widehat{a}$, $\widehat{b}$ and ϑ are computed from Eqs. S14 as a function of s. The predictions of the extended slender body theory are shown as continuous lines in Fig. 4d and Figs. 7a,b in the main text.

---

[1] A. O. Ivanov and O. B. Kuznetsova, *Phys. Rev. E*, 2001, **64**, 041405.

[2] A. F. Pshenichnikov, V. V. Mekhonoshin and A. V and Lebedev A.V., *J. Magn. Magn. Mater.*, 1996, **161**, 94–102.

[3] M. Suter, O. Ergeneman, J. Zürcher, S. Schmid, A. Camenzind, B. J. Nelson and C. Hierold, *J. Micromech. Microeng.*, 2011, **21**, 025023.

[4] C. Peters, O. Ergeneman, B. J. Nelson and C. Hierold, In: *Proc. IEEE Int. Conf. Micro Electro Mechanical Systems*, Taipei, Taiwan, 2013, pp. 564–567.

[5] K. I. Morozov and A. M. Leshansky, *Nanoscale*, 2014, **6**, 12142–12150.

[6] L. D. Landau and E. M. Lifshitz, *Electrodynamics of Continuous Media*, 2nd ed.; Pergamon Press, Oxford, 1984.

[7] W. F. Brown Jr., *Magnetostatic Principles in Ferromagnetism*; North-Holland, Amsterdam, 1962.

[8] The detailed analysis of the error introduced by the approximate representation of the MPC helix cross-section in Equation S13 is beyond the scope of the present analysis. It is fairly accurate for slender enough helices, such as those fabricated in Refs. [3, 4].